


Diphtheria toxin-derived, anti-PD-1 immunotoxin, a potent and practical tool to selectively deplete PD-1⁺ cells

Tianxiao Zhang¹ | Shuyun Dong¹ | Yujia Zhai¹ | Lauren Naatz¹ |
Zemin Zhou² | Mingnan Chen¹ 

¹Department of Molecular Pharmaceutics, University of Utah, Salt Lake City, Utah, USA

²Department of Pathology, University of Utah, Salt Lake City, Utah, USA

Correspondence

Mingnan Chen and Shuyun Dong,
Department of Molecular Pharmaceutics,
University of Utah, Salt Lake City, UT
84112, USA.

Email: mingnan.chen@utah.edu and
shuyun.dong@utah.edu

Funding information

HCI Melanoma Center Grant; National
Institutes of Health, Grant/Award
Number: AI139535; National Multiple
Sclerosis Society, Grant/Award Number:
GR-1807-31630

Review Editor: Aitziber L. Cortajarena

Abstract

Programmed death-1 (PD-1), an immune checkpoint receptor, is expressed on activated lymphocytes, macrophages, and some types of tumor cells. While PD-1⁺ cells have been implicated in outcomes of cancer immunity, autoimmunity, and chronic infections, the exact roles of these cells in various physiological and pathological processes remain elusive. Molecules that target and deplete PD-1⁺ cells would be instrumental in defining the roles unambiguously. Previously, an immunotoxin has been generated for the depletion of PD-1⁺ cells though its usage is impeded by its low production yield. Thus, a more practical molecular tool is desired to deplete PD-1⁺ cells and to examine functions of these cells. We designed and generated a novel anti-PD1 diphtheria immunotoxin, termed PD-1 DIT, targeting PD-1⁺ cells. PD-1 DIT is comprised of two single chain variable fragments (scFv) derived from an anti-PD-1 antibody, coupled with the catalytic and translocation domains of the diphtheria toxin. PD-1 DIT was produced using a yeast expression system that has been engineered to efficiently produce protein toxins. The yield of PD-1 DIT reached 1–2 mg/L culture, which is 10 times higher than the previously reported immunotoxin. Flow cytometry and confocal microscopy analyses confirmed that PD-1 DIT specifically binds to and enters PD-1⁺ cells. The binding avidities between PD-1 DIT and two PD-1⁺ cell lines are approximately 25 nM. Moreover, PD-1 DIT demonstrated potent cytotoxicity toward PD-1⁺ cells, with a half maximal effective concentration (EC₅₀) value of 1 nM. *In vivo* experiments further showed that PD-1 DIT effectively depleted PD-1⁺ cells and enabled mice inoculated with PD-1⁺ tumor cells to survive throughout the study. Our findings using PD-1 DIT revealed the critical role of pancreatic PD-1⁺ T cells in the development of type-1 diabetes (T1D). Additionally, we observed that PD-1 DIT treatment ameliorated relapsing–remitting experimental autoimmune encephalomyelitis (RR-EAE), a mouse model of relapsing–remitting multiple sclerosis (RR-MS). Lastly, we did not observe significant

Tianxiao Zhang and Shuyun Dong contributed equally.

hepatotoxicity in mice treated with PD-1 DIT, which had been reported for other immunotoxins derived from the diphtheria toxin. With its remarkable selective and potent cytotoxicity toward PD-1⁺ cells, coupled with its high production yield, PD-1 DIT emerges as a powerful biotechnological tool for elucidating the physiological roles of PD-1⁺ cells. Furthermore, the potential of PD-1 DIT to be developed into a novel therapeutic agent becomes evident.

KEYWORDS

autoimmune diseases, cancer, diphtheria toxin-derived immunotoxin, PD-1, programmed death-1 cells, protein therapeutics, yeast

1 | INTRODUCTION

The programmed death-1 (PD-1) protein was first identified and associated with apoptosis in 1992. Subsequently, PD-1 was recognized as a receptor sustaining the PD-1 immune checkpoint (Ishida, 2020; Patsoukis et al., 2020; Pauken et al., 2021). The checkpoint plays a crucial role in counterbalancing immune stimulatory signals and guiding the host away from autoimmunity and hyperimmunity. Lymphocytes that express PD-1 (referred to as PD-1⁺ lymphocytes) have become extensively utilized in cancer immunotherapy. In this approach, tumor-specific PD-1⁺ lymphocytes are re-energized through the blockade of the PD-1 checkpoint presented on these cells. Consequently, these rejuvenated lymphocytes exhibit enhanced antitumor immunity and eradicate tumor cells (Li et al., 2017). In addition to their roles in cancer immunity, PD-1⁺ lymphocytes, including primarily activated T and B lymphocytes, are also implicated in autoimmunity and chronic infections (Fife et al., 2009; Joller et al., 2012; Okazaki et al., 2013; Salama et al., 2003). Patients with rheumatoid arthritis (RA) have been found to possess elevated numbers of circulating PD-1⁺ lymphocytes. Furthermore, the majority of lymphocytes infiltrating the synovial tissues of RA patients are PD-1⁺ (Hosseinzadeh et al., 2021; Zhou et al., 2019). Additionally, disrupting the PD-1 immune checkpoint by knocking out PD-1 has been shown to worsen T1D in NOD mice and induce lupus-like phenotypes in C57BL/6 mice (Nishimura et al., 1999). Moreover, a blockade of the PD-1 immune checkpoint in NOD mice accelerates the onset of hyperglycemia (Ansari et al., 2003). Lastly, circulating T follicular regulatory lymphocytes (cTfr), which have increased PD-1 expression, contribute to the production and accumulation of high affinity autoantibodies (Hao et al., 2021; Huang et al., 2020; Xie et al., 2019). These findings highlight the significant involvement of PD-1⁺ lymphocytes in autoimmunity.

In addition to T and B lymphocytes, PD-1 has also been identified on various other immune cells,

including activated natural killer (NK) cells, macrophages, and innate lymphoid cells (Okazaki et al., 2013; Patsoukis et al., 2020). Interestingly, PD-1 was recently found to be expressed intrinsically by certain tumor cells. However, the role of these PD-1⁺ tumor cells in tumorigenesis and their impact on immune checkpoint therapy remain a topic of debate (Du et al., 2018; Kleffel et al., 2015; Wang et al., 2020; Wartewig et al., 2017; Yao et al., 2018). Some studies have demonstrated that PD-1 expressed on tumor cells suppress tumor growth (Du et al., 2018; Wang et al., 2020), whereas other data suggest that PD-1 may actually facilitate tumor growth (Kleffel et al., 2015; Schatton et al., 2010). In order to establish a clear understanding of the functions of PD-1⁺ cells in cancer, autoimmunity, and other pathological processes, a potential investigative strategy could involve studying effects of removing PD-1⁺ cells from these processes.

So far, a novel immunotoxin targeting PD-1 called α PD-1-ABD-PE has been developed by utilizing *Pseudomonas aeruginosa* exotoxin A (PE). This immunotoxin has demonstrated the ability to effectively deplete PD-1⁺ cells both in vitro and in vivo. This immunotoxin reduces PD-1⁺ cells in mouse models of EAE and T1D. These findings indicate that α PD-1-ABD-PE is a valuable tool for investigating the roles of PD-1⁺ cells in autoimmunity (Zhao et al., 2019). However, α PD-1-ABD-PE, produced using an *E. coli* expression system, faces a significant challenge in terms of low yield, typically generating only 0.1–0.2 mg from 1 L of culture. This limited yield greatly hinders the practicality of the immunotoxin, as exemplified by the case of OntakTM (denileukin diftitox), a clinically successful immunotoxin that was discontinued due to the production issues related to the *E. coli* expression system (Shafiee et al., 2019). Consequently, we have undertaken the development of a new immunotoxin, coupled with a suitable expression system. Our objective is to enhance the production yield of anti-PD-1 immunotoxin and improve the overall feasibility of this molecular

tool for elucidating the roles of PD-1⁺ cells in different pathological processes.

Since the 1970s, diphtheria toxin (DT) has been extensively investigated as a therapeutic agent (Moolten & Cooperband, 1970). Currently, two protein drugs derived from diphtheria toxin, Ontak™ and Tagraxofusp™, have received clinical approval (Shafiee et al., 2019). In 1985, Murphy's group made significant advancement producing diphtheria toxin-containing proteins through the yeast expression system (*Saccharomyces cerevisiae*) (Chen et al., 1985; Perentesis et al., 1988). Later, in 2002, Neville's group successfully generated a diphtheria toxin-containing immunotoxin using the yeast strain, *Pichia pastoris* GS115, achieving a yield of about 10 mg/L. (Woo et al., 2002) This study highlighted the greater tolerance of *Pichia pastoris* exhibit to diphtheria toxin compared to *S. cerevisiae*. *Pichia pastoris*, developed by Cregg's group in the 1980s, offers distinct advantages such as using strong and regulatable promoters and integrating coding genes into the genome of *Pichia pastoris* (Cregg et al., 1985; Gellissen, 2000). These advantages, coupled with yeast's rapid growth and cost-effective culture, make yeast an appealing expression system for diphtheria toxins. Notably, after Ontak was discontinued due to its production by the *Escherichia coli* expression system in 2014 (Wang et al., 2017), a bivalent Ontak-like protein (DAB389-IL2IL2) was successfully produced in *Pichia pastoris*. This new protein exhibited 100-fold stronger cytotoxicity (Shafiee et al., 2019). This new development further supports the utility of *Pichia pastoris* for producing diphtheria toxin-based immunotoxins.

We present a novel diphtheria immunotoxin in this study, referred to as PD-1 DIT, which specifically targets PD-1⁺ cells. PD-1 DIT consists of a truncated diphtheria toxin that is fused with two copies of anti-PD-1 antibody scFvs. By employing *Pichia pastoris* GS115, we have successfully produced PD-1 DIT with a high yield of 1.0–2.0 mg/L culture media. PD-1 DIT exhibits strong binding affinity to PD-1⁺ cells, and once bound, it is internalized by these cells. We have observed remarkable efficacy in selectively depleting PD-1⁺ cells both in vitro and in vivo. Notably, PD-1 DIT effectively eliminated transferred EL4 lymphoma cells, resulting in the survival of all mice that received the transfer and treatment. Moreover, we investigated the impact of PD-1 DIT treatment on the infiltration of PD-1⁺ cells into pancreatic islets of NOD mice, a well-established mouse model for spontaneous T1D. The results demonstrated a reduction in the number of PD-1⁺ cells infiltrating the pancreatic islets upon treatment with PD-1 DIT. Additionally, we evaluated the therapeutic potential of PD-1 DIT in animal models of both T1D and MS (multiple sclerosis), where we observed positive effects on the progression of these diseases.

Importantly, PD-1 DIT does not cause liver damage, a common side effect associated with immunotoxins derived from diphtheria toxin. This finding suggests that PD-1 DIT is a safe molecular tool suitable for preclinical investigations. In summary, PD-1 DIT represents a powerful and practical approach for depleting PD-1⁺ cells and holds promise as a potential therapeutic agent for autoimmune diseases and cancers.

2 | RESULTS

2.1 | Design and generation of anti-PD-1 diphtheria immunotoxin (PD-1 DIT)

We previously demonstrated that the targeted depletion of PD-1⁺ cells using an immunotoxin effectively slowed down or even reversed the progression of specific autoimmune diseases (Zhao et al., 2019). However, the previous immunotoxin has limitations due to its low yield. To address this issue and enhance production efficiency, we designed a novel immunotoxin called PD-1 diphtheria immunotoxin (PD-1 DIT). PD-1 DIT incorporates two functional components from the NH₂-terminus to the COOH-terminus, namely a truncated diphtheria toxin and scFvs derived from an anti-mouse PD-1 antibody, (the RMP1-14 clone; Figure 1a) (Mirdita et al., 2022; Zhao et al., 2019). This design, which places the toxin at the NH₂ side of the scFvs and keeps the catalytic domain of the toxin (Cyan, Figure 1a) at the NH₂-terminus of PD-1 DIT, bears resemblance to the natural domain arrangement of diphtheria toxin (PDB: 1SGK). The importance of such design has been demonstrated by studies of other immunotoxin derived from diphtheria toxin (Auger et al., 2015). The design of the toxin component is intricate and will be explained in more details in the following paragraph. On the other hand, the scFv component consists of two identical scFvs arranged in a bivalent tandem configuration, a design that has been shown to enhance the binding affinity and potency of immunotoxins (Reiter et al., 1994; Thompson et al., 2001). Each scFv starts with the variable domain of the anti-PD-1 antibody light chain, followed by the variable domain of the anti-PD-1 antibody heavy chain. A peptide linker, (GGGGS)₃, is utilized to connect between the variable domains of scFvs as well as between two scFvs (Pink, Figure 1a). Another linker, GGGGS, is used as a spacer between the toxin and the scFv components (Purple, Figure 1a).

The truncated diphtheria toxin utilized in PD-1 DIT consists of the initial 1–390 residues of diphtheria toxin (Liu et al., 2000). Within this structure, residues 1–187 form the catalytic domain (Cyan); residues 200–390 form the translocation domain (Cornflower blue); and residues

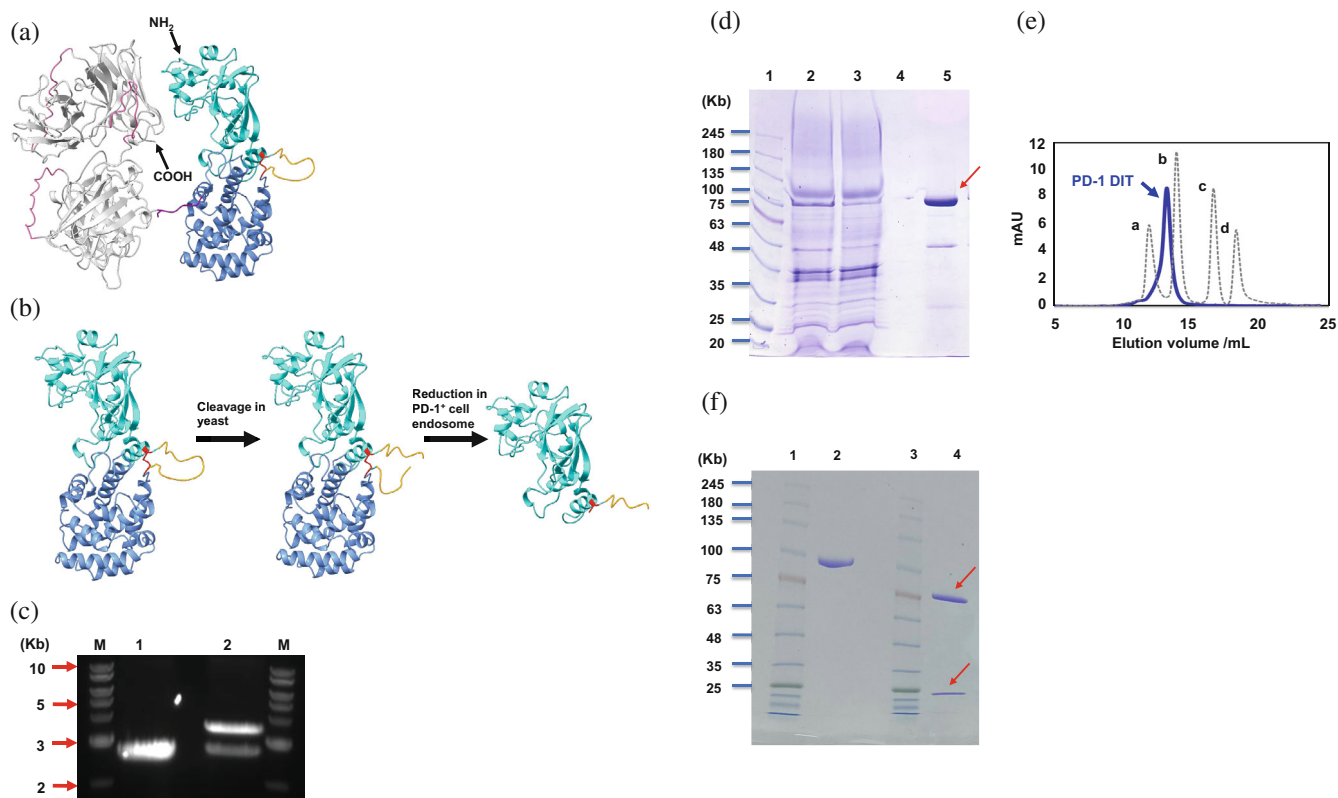


FIGURE 1 Design and production of PD-1 DIT. (a) A predicted structure of PD-1 DIT. Within PD-1 DIT, the truncated diphtheria toxin (PDB: 1sgk) consists of a catalytic domain (cyan) and a translocation domain (cornflower blue); the two domains are connected by a disulfide bond (red) and a loop (GNRVRRSVGSSL, yellow). Two anti-mouse PD-1 scFvs (gray) are arranged in tandems, with pink-colored linkers connect the light and heavy chains of the scFvs, and between two scFvs. There is also a linker (purple) connecting the toxin and the anti-PD-1 scFvs. (b) A series of schematic illustration demonstrating the separation of the catalytic domain from the translocation domain of the toxin and the rest of PD-1 DIT. The first step involves the cleavage of the loop (yellow); the second step involves the reduction of the disulfide bond (red). (c) An agarose gel photograph showing the coding gene of PD-1 DIT (Lane 1) and the double-digestion products of the expression plasmid (Lane 2). In the lane 2, the upper band is the vector backbone, and the lower band is the coding gene of PD-1 DIT. (d) An SDS-PAGE gel image illustrating collected samples at different steps of PD-1 DIT purification. Lane 1, protein ladder. Lane 2, cell culture medium which contains PD-1 DIT. Lane 3, unbound proteins flowing off from a nickel column. Lane 4, residue proteins on the nickel column after proteins are eluted. Lane 5, eluted proteins (the red arrow is pointed to PD-1 DIT). (e) The peak of PD-1 DIT on size exclusion chromatography. Protein standards a, b, c, and d are β -Amylase (150 kDa), bovine serum albumin (66 kDa), carbonic anhydrase (29 kDa), and cytochrome c (12.4 kDa), respectively. (f) An SDS-PAGE gel photograph showing PD-1 DIT in reduced and nonreducing states. Lane 1, protein ladder. Lane 2, PD-1 DIT in the nonreducing state. Lane 3, protein ladder. Lane 4, PD-1 DIT in the reduced state. In the lane 4, the upper arrow indicates PD-1 DIT without the catalytic domain, while the lower arrow points to the catalytic domain.

188–199 (GNRVRRSVGSSL) form a loop between the two domains (Orange, Figure 1b, Left). After the initial translation and folding, the catalytic domain and translocation domains are joined by both the loop and an inter-domain disulfide bond (Red, Figure 1b, Left). Subsequently, the loop is cleaved within yeast cells, resulting in purified PD-1 DIT containing two domains linked solely by the disulfide bond (Figure 1b, Middle). The cleavage within the loop of PD-1 DIT is favored for its cytotoxicity because the process enables the release of the catalytic domain and conversion of the toxin component from a pro-enzyme to an enzyme (Figure 1b, Right) (Bennett et al., 1994; Collier, 2001; Williams et al., 1987).

The cleavage also makes the catalytic domain ready to translocate into the cytosol to inhibit protein synthesis (Becker & Benhar, 2012; Shapira & Benhar, 2010; Varkouhi et al., 2011).

A *Pichia pastoris* strain GS115 was selected for the expression of PD-1 DIT. A coding gene of PD-1 DIT was inserted into the pPICZa B plasmid to utilize this yeast expression system (Figure S1). A coding gene for α secretory factor signal was fused to the 5'-end of the PD-1 DIT gene. The successful insertion of the PD-1 DIT gene was confirmed by the examination of the XhoI/XbaI double digestion products of the resulting plasmid through an agarose gel electrophoresis (Figure 1c). The authenticity

of PD-1 DIT gene and its insertion site were further verified by DNA sequencing. The resulting protein, PD-1 DIT, was purified using Ni-NTA affinity chromatography (Figure 1d) and subsequently size exclusion chromatography (SEC) (Figure S2). The purity of the purification product was assessed by SEC (Figure 1e). On the SDS-PAGE, nonreduced, purified PD-1 DIT migrated as a band close to the protein marker of 100 kDa, consistent with the theoretical molecular weight of PD-1 DIT, 98 kDa (Lane 2, Figure 1f). On the other hand, reduced, purified PD-1 DIT migrate on SDS-PAGE as two distinct bands at approximately 25 kDa and 75 kDa, respectively (Lane 4, Figure 1f). The 25 kDa band corresponds to the catalytic domain while the 75 kDa band represents the rest of PD-1 DIT. The presence of these two bands confirmed the idea that the catalytic domain is linked with the rest of PD-1 DIT through a disulfide bond (Figure 1b, Right). The yield of PD-1 DIT is approximately 1–2 mg/L, which is 10 times higher than the yield of α PD-1-ABD-PE used in our previous study (Zhao et al., 2019).

2.2 | Binding and internalization of PD-1 DIT

The binding and internalization of PD-1 DIT to PD-1⁺ cells were first examined by flow cytometry. Specifically, Alexa Fluor 647-labeled PD-1 DIT was incubated with EL4 cells, which are a PD-1⁺ cell line, at 37°C for varying durations up to 4 h. Mean fluorescence intensities (MFIs) of these EL4 cell samples were then determined. A significant increase in MFIs is observed from the 0-h incubation samples to the 4-h incubation samples. This trend is consistent across two different concentrations of PD-1 DIT concentrations, namely 1.0 and 2.5 μ g/mL (Figure 2a,b). Furthermore, for a given incubation time, a higher concentration of PD-1 DIT resulted in higher MFIs (Figure 2c). These findings suggest that the binding and internalization are dependent on both concentration and time. Additionally, MFIs of EL4 cells that were incubated at 37°C and 4°C were measured and compared. Incubation at 4°C is known to impede cellular internalization. When 1.0 μ g/mL PD-1 DIT was used for the study, cell samples incubated at 37°C exhibited MFIs over two times higher than those incubated at 4°C for all three incubation periods used (0.5 h: 969.0 \pm 26.6 vs. 362.3 \pm 14.1; 2 h: 1985.7 \pm 19.3 vs. 570.3 \pm 64.8; 4 h: 2714.7 \pm 46.4 vs. 1124.3 \pm 10.3; $p < 0.0001$ for all incubations, Figure 2d). The superiority of the 37°C incubation was also evident when 2.5 μ g/mL PD-1 DIT was used (0.5 h: 2458.7 \pm 86.1 vs. 656.7 \pm 12.9; 2 h: 4798.7 \pm 83.5 vs. 968.3 \pm 127.4; 4 h: 5545.7 \pm 181.3 vs. 2106.0 \pm 85.5,

$p < 0.0001$ for all incubations, Figure 2e). The superiority suggests that a fraction of PD-1 DIT is internalized by EL4 cells at 37°C. Additionally, the binding between PD-1 DIT and PD-1⁺ cells was evaluated in a quantitative manner using a cell-based direct binding assay (Hunter & Cochran, 2016; Moore & Cochran, 2012). This assay enables the determination of avidity between proteins and cells that express their binding partners on cell surfaces. Two types of PD-1⁺ cells, EL4 and 2D2, which have slightly but noticeably different PD-1 expression levels, were employed (Figure S3). EL4 cells demonstrated slightly higher avidity compared to 2D2 cells. The binding EC₅₀ for EL4 was determined to be 25.7 \pm 0.7 nM, whereas the binding EC₅₀ for 2D2 was 27.3 \pm 0.9 nM (Figure S4).

To further analyze the interactions between PD-1 DIT and PD-1⁺ cells, we employed confocal laser scanning microscopy (CLSM) to examine cells after incubating them with PD-1 DIT. Specifically, Alexa Fluor 647-labeled PD-1 DIT was incubated for 10 h with EL4 or EL4 (PD-1^{KO}) cells that lack PD-1 expression. PD-1 DIT was found to associate with EL4 cells based on the Alexa Fluor 647 emission signal (Figure 3a–d). A significant amount of PD-1 DIT was observed to associate with the cell membrane stained with WGA555 (Figure 3a,b). Further, some signals of Alexa Fluor 647 were also spotted inside the cell membrane (Figure 3d, pointed by arrows). In contrast, no detectable signal was observed in association with EL4 (PD-1^{KO}) cells (Figure 3e–h). Similarly, neither EL4 (Figure 3i–l) nor EL4 (PD-1^{KO}) (Figure 3m–p) cells exhibited any signals of Alexa Fluor 647 when they were not incubated with PD-1 DIT. These findings strongly suggest that the signals of Alexa Fluor 647 are a result of the Alexa Fluor 647-labeled PD-1 DIT selectively binding to and being internalized into PD-1⁺ cells. Furthermore, the binding and internalization of PD-1 DIT into EL4 cells are time dependent within the 10 h incubation period. The signals associated with EL4 cells became stronger as the incubation time increased from 0.5 h to 2 h, and finally to 10 h (Figure S5). In contrast, no detectable signals were observed at any of these time points when EL4 (PD-1^{KO}) cells were used for the study.

We further analyzed PD-1 DIT associated with cells in confocal images using a quantification method outlined in Figure S6. The mean intensity value per cell (MIVpC) of Alexa Fluor 647 associated with EL4 cells was found to be significantly higher than that with EL4 (PD-1^{KO}) cells after both cell lines were incubated with PD-1 DIT for 10 h (Figure 3q). Meanwhile, without the PD-1 DIT incubation, both cell lines exhibited low MIVpCs. MIVpCs of EL4 cells significantly increased when cells were incubated with PD-1 DIT for longer time

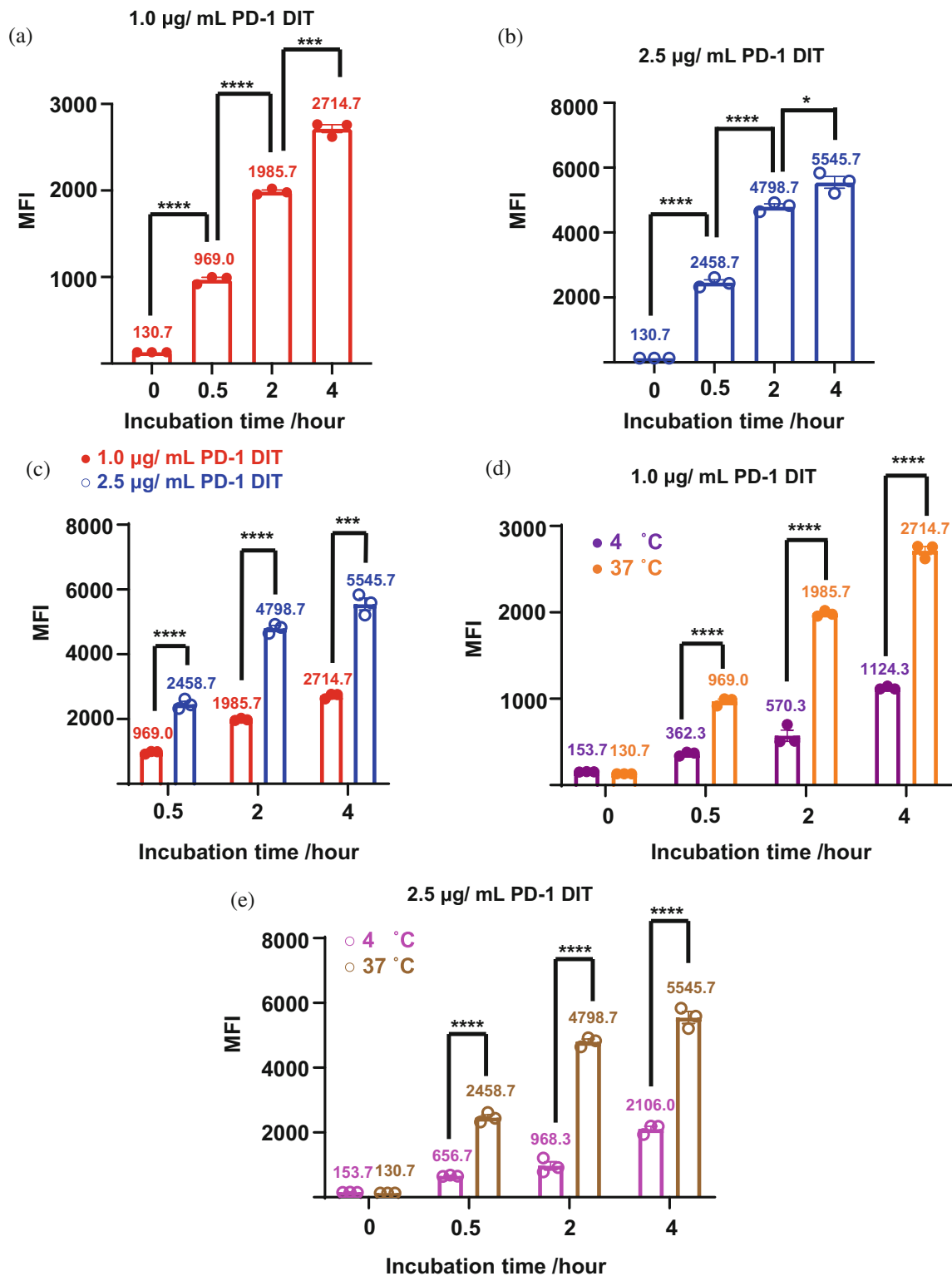


FIGURE 2 The characterization of the cellular association of PD-1 DIT by flow cytometry. (a) The mean fluorescence intensity (MFI) of EL4 cells after incubation with Alexa Fluor 647-labeled PD-1 DIT (1.0 $\mu\text{g}/\text{mL}$). The mean MFL values for each treatment are labeled ($N = 3$). (b) The MFI of EL4 cells after incubation with Alexa Fluor 647-labeled PD-1 DIT (2.5 $\mu\text{g}/\text{mL}$). The mean MFL values for each treatment are labeled ($N = 3$). (c) Comparisons of mean MFIs between EL4 cells incubated with 1.0 $\mu\text{g}/\text{mL}$ and 2.5 $\mu\text{g}/\text{mL}$ of PD-1 DIT. The mean MFL values for each treatment are labeled ($N = 3$). (d) Comparison of mean MFI values between EL4 cells after they are incubated with PD-1 DIT (1.0 $\mu\text{g}/\text{mL}$) at 4°C and 37°C, respectively. The mean MFL values for each treatment are labeled ($N = 3$). (e) Comparison of mean MFI values between EL4 cells after they are incubated with PD-1 DIT (2.5 $\mu\text{g}/\text{mL}$) at 4°C and 37°C, respectively. The mean MFL values for each treatment are labeled ($N = 3$). (Statistical significance is indicated by asterisks: * $p < 0.05$, *** $p < 0.001$, **** $p < 0.0001$.)

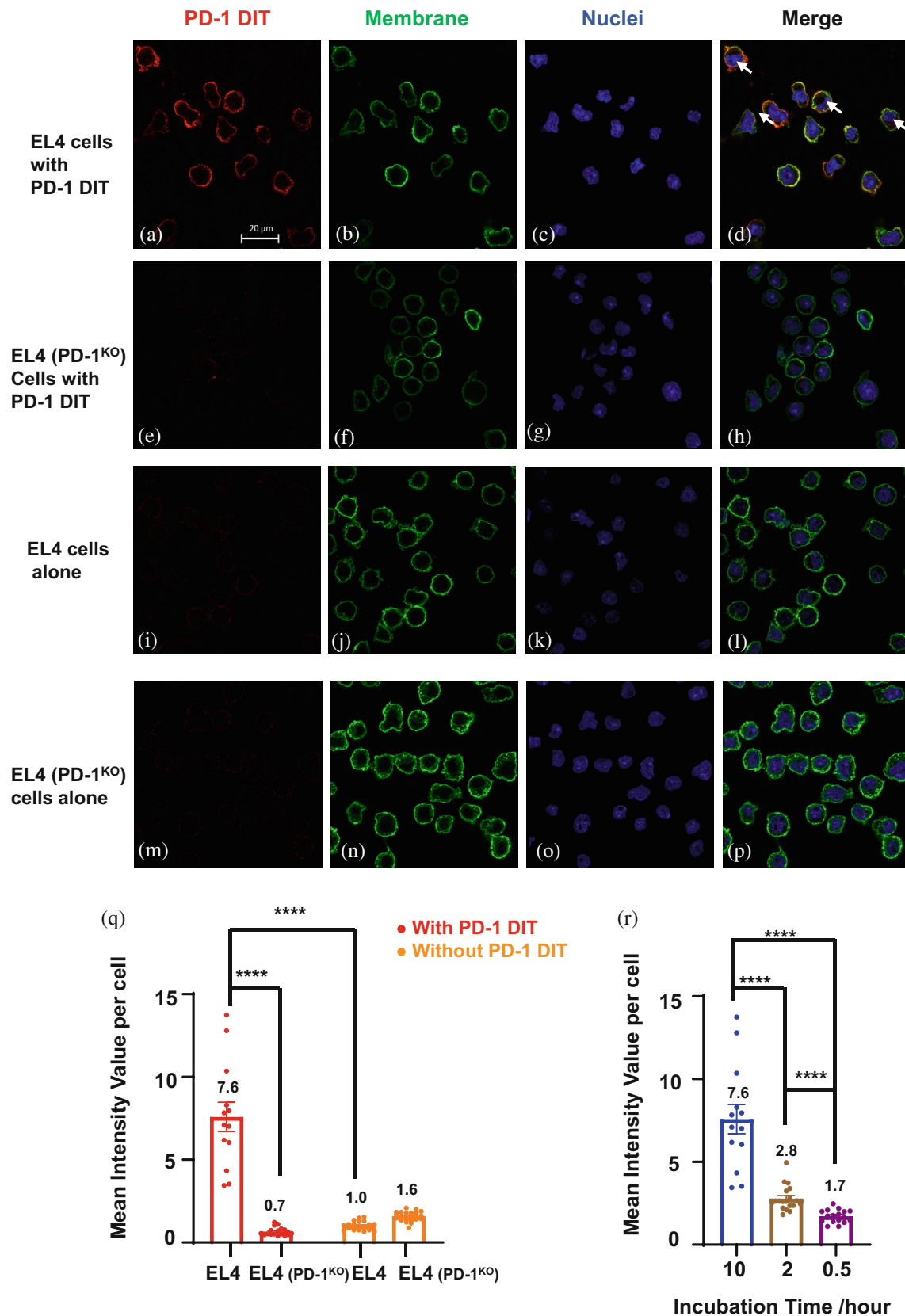


FIGURE 3 The characterization of the cellular association of PD-1 DIT by confocal microscopy. (a–d) Confocal images of EL4 cells and (e–h) EL4 (PD-1^{KO}) cells after incubation with Alexa Fluor 647-labeled PD-1 DIT for 10 h. (i–l) Confocal images of EL4 cells and (m–p) EL4 (PD-1^{KO}) cells after incubation with cell culture media only for 10 h. Color code is as follows: red represents PD-1 DIT; green represents cell membrane; blue represents nuclei. A scale bar of 20 μ m is provided for reference. (q) Mean intensity value per cell (MIVpC) after cells were incubated with or without labeled PD-1 DIT for 10 h. The data are expressed as mean \pm SEM ($N > 12$ cells for each group). (r) Mean intensity value per cell (MIVpC) after EL4 cells were incubations with labeled PD-1 DIT for 0.5, 2, and 10 h. The data are expressed as mean \pm SEM ($N > 12$ cells for each group).

(Figure 3r). Taken together, the results obtained from confocal microscopy provide conclusive evidence that PD-1 DIT exhibits selective binding and internalization into PD-1⁺ cells.

2.3 | In vitro and in vivo cytotoxicity of PD-1 DIT

The cytotoxicity of PD-1 DIT was examined in vitro using three cell types, EL4 cells, 2D2 cells, and EL4 (PD-1^{KO}) cells. The EC₅₀ values of PD-1 DIT are 0.4 nM, 1 nM, and over 1 μM for EL4, 2D2, and EL4 (PD-1^{KO}) cells, respectively, according to a 72-h cytotoxicity assay (Figure 4a). This indicates, EL4 and 2D2 cells are at least a thousand times more sensitive to PD-1 DIT than EL4 (PD-1^{KO}) cells. Results from a 24-h cytotoxicity assay further demonstrated that PD-1 DIT effectively depletes PD-1⁺ cells as soon as 24 h (Figure 4b). These findings establish that PD-1⁺ cells with varying levels of PD-1 expression are

sensitive to the cytotoxicity of PD-1 DIT yet the cytotoxicity is PD-1⁺ cell-specific, conforming the validity of the immunotoxin's design. To validate the functionality of the anti-PD-1 scFvs in our immunotoxin, we compared the cytotoxicity of PD-1 DIT and another diphtheria-derived immunotoxin that is comprised of bivalent tandem anti-human CD3 scFvs (CD3 DIT), using EL4 cells as the test subject. The study revealed an EC₅₀ value of 1.4 nM for PD-1 DIT, while the EC₅₀ of the CD3 DIT was not achieved even at a concentration of 100 nM (Figure 4c). This result reinforces the targeting role of anti-PD-1 scFvs in PD-1 DIT.

The cytotoxicity of PD-1 DIT was subsequently examined in vivo using an EL4 cell transfer model. EL4, a type of T lymphoblast tumor cells (Zhao et al., 2019), were injected into mice, and these mice were then randomized into two groups: one receiving PBS treatment while the other receiving PD-1 DIT treatment. The dose of PD-1 DIT is determined according to its maximum tolerated dose (MTD), 0.75 mg/kg (unshown data and Figure S7).

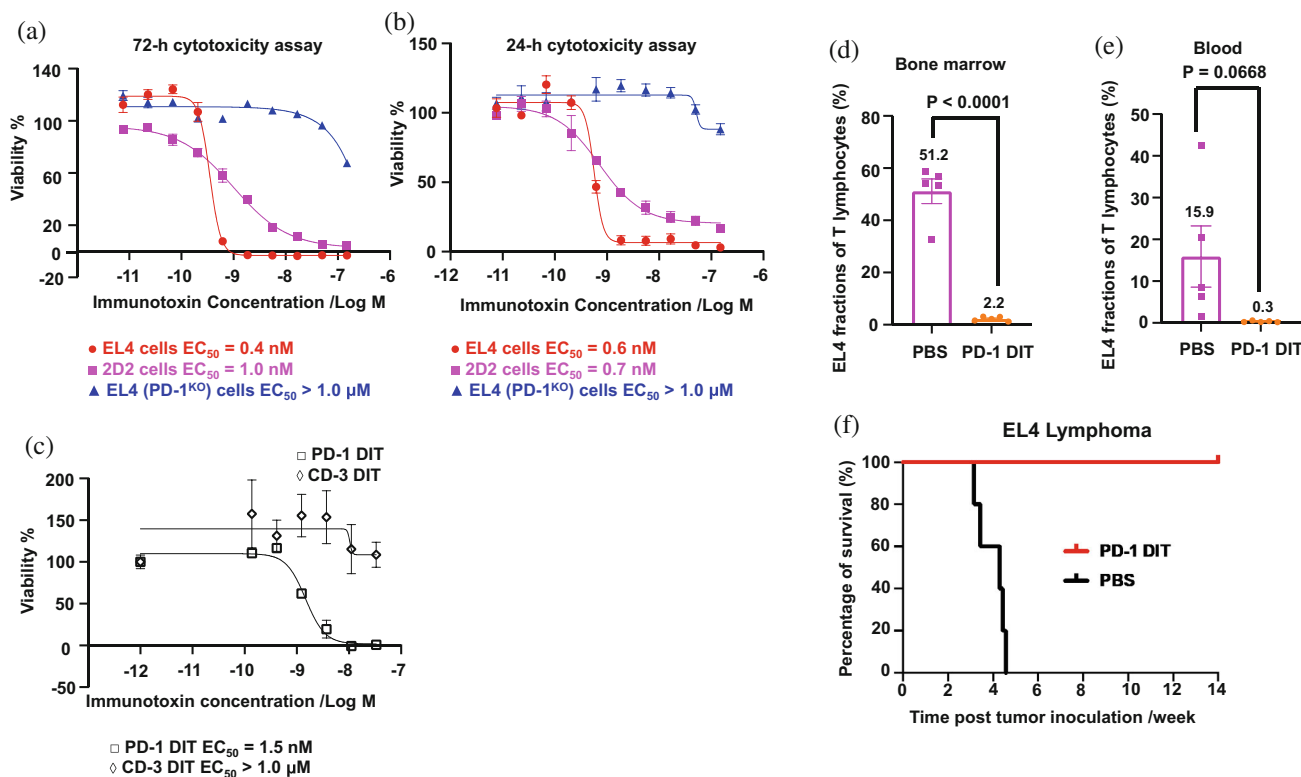


FIGURE 4 Depletion of PD-1⁺ cells by PD-1 DIT. (a) Viability of EL4, 2D2, and EL4 (PD-1^{KO}) cells after incubation with PD-1 DIT for 72 h. The viability values are presented as mean ± SEM at various concentrations of PD-1 DIT ($N = 3$). The data were fitted to the sigmoidal dose–response (variable slope) model. (b) Viability of EL4, 2D2, and EL4 (PD-1^{KO}) cells after incubation with PD-1 DIT for 24 h. The viability values are presented as mean ± SEM ($N = 3$). The data were fitted to the sigmoidal dose–response model. (c) Viability of EL4 cells after incubation with PD-1 DIT or CD-3 DIT for 72 h. The viability values are shown as mean ± SEM ($N = 3$). The data were fitted to the sigmoidal dose–response model. (d) Fractions of EL4 cells among T lymphocytes collected from the bone marrow of mice 72 h after the last dose of treatment. The data are presented as mean ± SEM ($N = 5$ mice). (e) Fraction of EL4 cells among T lymphocytes collected from the blood of mice 72 h after the last dose of treatment. The data are presented as mean ± SEM ($N = 5$ mice).

A total of five doses of either PBS or PD-1 DIT were administered, beginning 1 day after the cell transfer. On day 12 following the cell transfer, we analyzed T cells in bone marrow since EL4 cells have a tendency to accumulate in this tissue (Zhai et al., 2022). Our findings demonstrated that the PD-1 DIT treatment significantly reduced EL4 cell fraction (PD-1⁺ T cells) among T cells (CD3⁺) in the bone marrow as compared to the PBS treatment ($2.2 \pm 0.4\%$ vs. $51.2 \pm 4.8\%$, $p < 0.0001$, Figure 4d). In fact, the cell fraction was reduced by approximately 25 times. Moreover, the depletion effect of PD-1 DIT was observed among T cells in the blood as well (Figure 4e). The mean EL4 fraction among circulating T cells in the PD-1 DIT treatment group is $0.3 \pm 0.1\%$, while it was $15.9 \pm 7.3\%$ in the PBS treatment group. The depleting effect of PD-1 DIT also had a positive impact on the overall survival of mice that received EL4 cell transfer. The median survival time for PBS treated group were only 30 days after tumor inoculation, whereas all mice treated with PD-1 DIT remained alive at the end of the study (>100 days) (Figure 4f). The survival of PD-1 DIT-treated mice was significantly prolonged compared to the PBS-treated mice ($p < 0.01$). These results further confirm the potent depleting activity of PD-1 DIT in vivo and suggest the potential investigational and therapeutic applications of the immunotoxin.

2.4 | Role of PD-1⁺ lymphocytes in T1D revealed by using PD-1 DIT

NOD mice exhibit spontaneous development of T1D. Female mice have the infiltration of PD-1⁺ lymphocytes into their pancreatic islets by the age of 9 weeks (Liang et al., 2003). In fact, approximately 80% of CD4 and CD8 T effector lymphocytes present in the pancreatic islets of female NOD mice are PD-1⁺ when these mice at 10 weeks of age, according to our observation (Figure S8). We thus examined whether the treatment of PD-1 DIT ablates these PD-1⁺ lymphocytes. Our results demonstrated that PD-1 DIT treatment led to a reduction in PD-1⁺ CD4 T lymphocytes. The mean of PD-1⁺ CD4 T lymphocytes per islet in the PD-1 DIT-treated mice was 68.6 ± 27.7 , while in PBS treated mice, it was 155.3 ± 46.0 (Figure 5a). A similar trend was observed for PD-1⁺ CD8 T lymphocytes (PD-1 DIT: 9.3 ± 6.2 vs. PBS: 13.6 ± 5.5). Additionally, when evaluating CD4 and CD8 T effector lymphocytes, PD-1⁺ effector lymphocytes were also reduced by PD-1 DIT treatment (CD4 T effector lymphocytes: 61.1 ± 24.8 vs. 138.4 ± 41.5 ; CD8 T effector lymphocytes: 7.6 ± 5.2 vs. 9.9 ± 4.3 , Figure 5b). In addition, there was a noticeable reduction of PD-1⁺ CD44⁺CD62L⁺ CD4 and CD8 lymphocytes following

PD-1 DIT treatment (Figure 5c). PD-1⁺ cells account for 30%–50% of CD44⁺CD62L⁺ CD4 and CD8 T lymphocytes, which are much smaller than their fractions within in effector lymphocytes (Figure S8). Meanwhile, T effector cells are dominant subpopulation among all PD-1⁺ T cells (Figure S9).

We then used PD-1 DIT to investigate the impact of PD-1⁺ cells on the progression of T1D. We selected a T1D model characterized by an accelerated progression of hyperglycemia driven by PD-1 immune checkpoint blockade (Zhao et al., 2019). In this study, both male and female mice were pretreated with five doses of PD-1 DIT or PBS (Figure 5d). Subsequently, all mice received treatment of a blocking anti-PD-1 antibody to initiate PD-1 immune checkpoint blockade. The administration of the blocking antibody swiftly induced hyperglycemia in mice pretreated with PBS, indicating the reactivation of autoreactive diabetogenic PD-1⁺ cells by the blockade treatment. In contrast, pretreatment with PD-1 DIT significantly delayed the onset of hyperglycemia. Remarkably, male mice pretreated with PD-1 DIT remained normoglycemic throughout the entire study (Figure 5e). These findings suggest that PD-1 DIT reduces the population of diabetogenic PD-1⁺ cells, thereby rendering the PD-1 blockade treatment ineffective due to the loss of its cellular target. Notably, the effect of PD-1 DIT was more pronounced in male mice than in female mice, which differs from the observations reported in other studies. This difference may be attributed to the higher degree of insulinitis and lymphocyte infiltration experienced by female mice of this age (Fife et al., 2006; Young et al., 2009). Collectively, these results indicate the fundamental role PD-1⁺ cells in the onset and progression of T1D.

2.5 | Roles of PD-1⁺ lymphocytes in RR-EAE revealed by using PD-1 DIT

We employed PD-1 DIT and its ability to deplete PD-1⁺ lymphocytes to investigate the roles of PD-1⁺ lymphocytes in another autoimmune disease model, RR-EAE. This model closely resembles relapsing–remitting multiple sclerosis (RR-MS), which accounts for 85% of MS case (Hammer et al., 2013; National Multiple Sclerosis Society, 2013). RR-EAE was induced in SJL/J mice, and PD-1 DIT treatment was initiated 3 days after EAE induction (Black arrows indicate the treatment of PD-1 DIT, Figure 5g). PD-1 DIT treatment effectively suppressed the development of EAE during the relapsing phase (Day 21–26 after induction). The average clinical score of mice in the PD-1 DIT-treated group was notably lower throughout the study, highlighting the therapeutic effect of PD-1 DIT in ameliorating RR-EAE disease. These findings

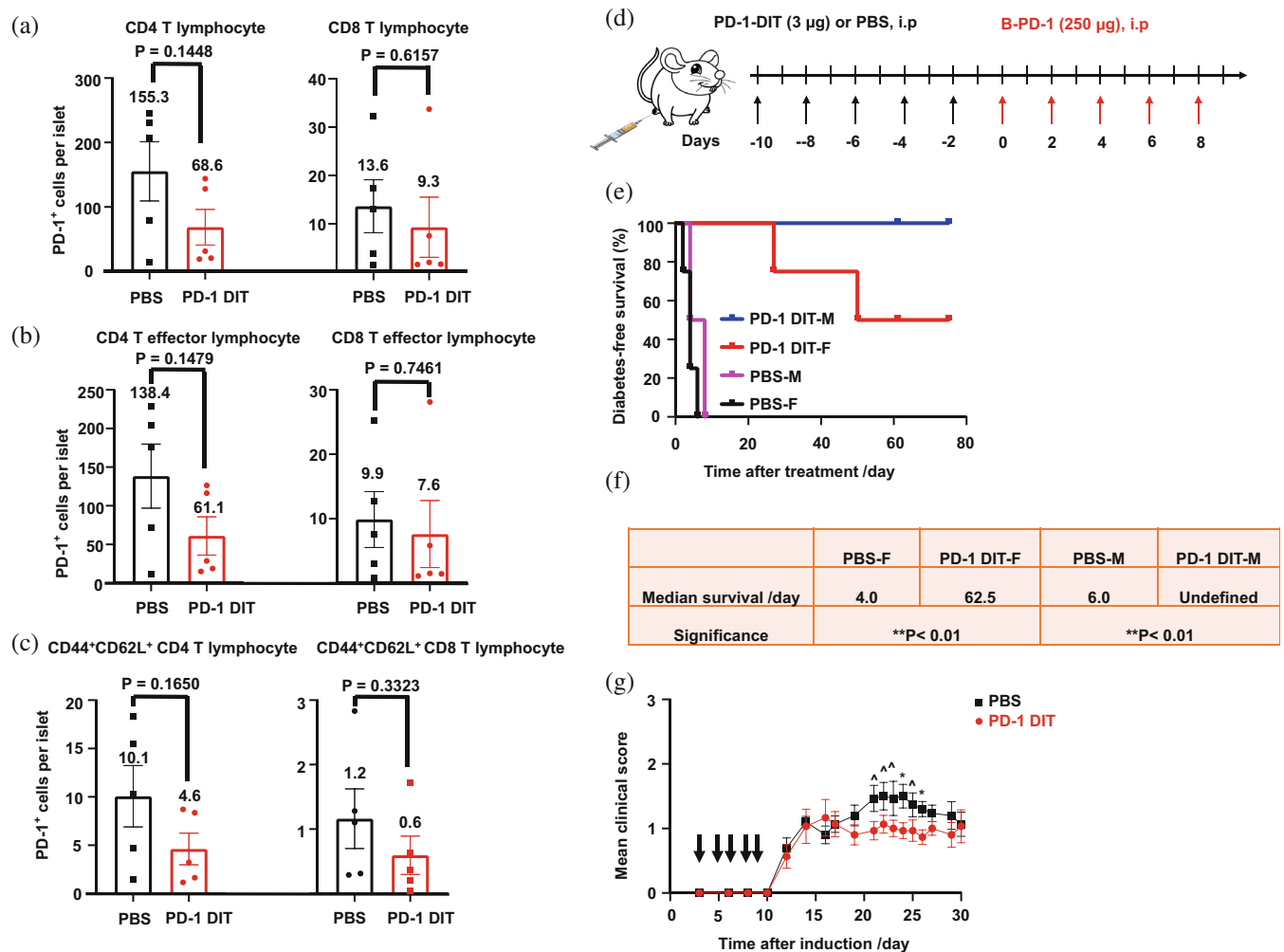


FIGURE 5 PD-1 DIT treatment delays the onset of T1D. (a) Numbers of PD-1⁺ CD4 and CD8 T lymphocytes per islet in mice receiving PBS or PD-1 DIT treatments. The data are presented as mean \pm SEM ($N = 5$ mice). (b) Numbers of PD-1⁺ CD4 and CD8 T effector lymphocytes per islet in mice receiving PBS or PD-1 DIT treatments. The data are presented as mean \pm SEM ($N = 5$ mice). (c) Numbers of PD-1⁺ CD44⁺CD62L⁺ CD4 and CD8 T lymphocytes per islet in mice receiving PBS or PD-1 DIT treatments. The data are presented as mean \pm SEM ($N = 5$ mice). (d) An illustrative figure depicting the study design to investigate the impact of PD-1⁺ cells on the progression of T1D. NOD mice received 5 doses of PD-1 DIT or PBS once every 2 days before day 0 (black arrows). From Day 0, the mice were given 5 doses of blocking anti-PD-1 antibodies (B- α PD-1) once every 2 days (red arrows). (e) Diabetes-free survival of NOD mice in the study described in (d) ($N = 4$ mice). Female (F) and male (M) NOD mice were divided into two groups and received pretreatment of PBS and PD-1 DIT, respectively. (f) Median diabetes-free survival days of each treatment groups in the study described in (d). The Logrank tests were used to examine difference between the PD-1 DIT-F and PBS-F groups, and between the PD-1 DIT-M and PBS-M groups. (g) Clinical scores of SJL/J mice with RR-EAE that were treated with PD-1 DIT (red dot) or PBS (black square). The black arrow indicates the day of treatments. The data at each observation day are presented as mean \pm SEM ($N = 15$ mice). (* $p < 0.05$; “^” the mean clinical scores of the two groups are apparently but not significantly different; unpaired two-tailed t -test.)

strongly indicate that PD-1⁺ cells contribute to the occurrence of relapses in RR-EAE.

2.6 | Hepatotoxicity assessment of PD-1 DIT

Hepatotoxicity has been observed in clinical trials for diphtheria toxin-derived immunotoxins (Mei et al., 2019).

However, it is unclear whether the hypertoxicity is universal among this type of immunotoxins or the toxicity varies depending on antigens targeted by the immunotoxins. Therefore, it is worthwhile investigating whether PD-1 DIT, which targets PD-1⁺ cells, leads to significant hypertoxicity. We assessed hepatotoxicity by measuring serum levels of alanine aminotransferase (ALT) and aspartate aminotransferase (AST) (Salaspuro, 1987) as higher than normal levels of ALT and AST indicate

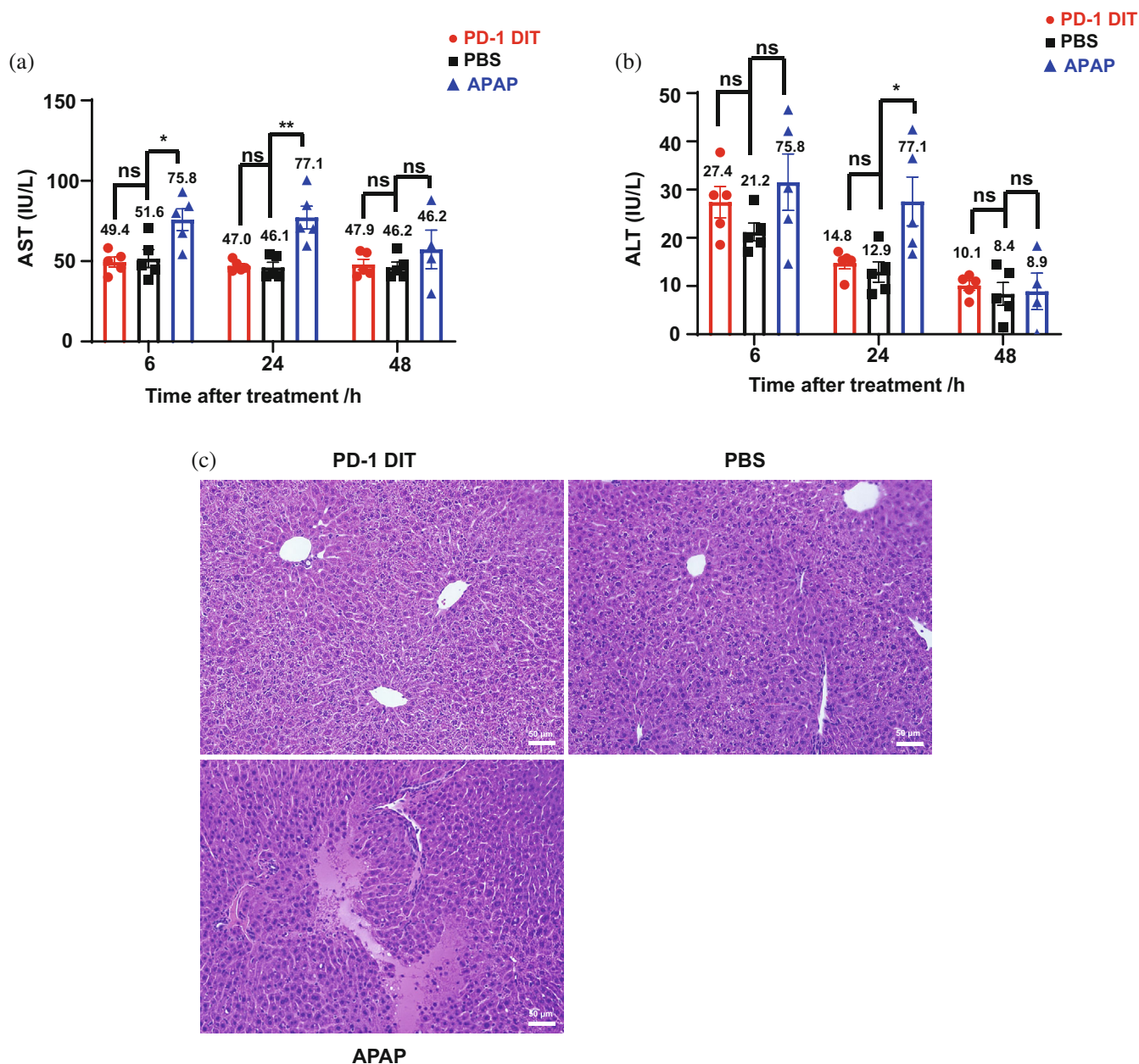


FIGURE 6 Hepatotoxicity assessment of PD-1 DIT. (a) Serum AST levels in mice treated with PD-1 DIT, PBS, or APAP, respectively. Values are presented as means \pm SEM ($N = 5$ mice). (b) Serum ALT levels in mice treated with PD-1 DIT, PBS, or APAP, respectively. Values are presented as means \pm SEM ($N = 5$ mice). (c) Photos of liver tissue sections. The three photographed areas represent multiple view areas from 15 tissue sections from the PD-1 DIT, PBS, and APAP-treated groups, respectively. The main features in the photos were consistent with other view areas we observed. The scale bar is 50 μ m. (Statistical significance is indicated by asterisks: * $p < 0.05$; ** $p < 0.01$; ns: not significant.)

hepatotoxicity. Mice were randomized into three groups receiving PBS, PD-1 DIT (0.375 mg/kg body weight), and acetaminophen (APAP, 450 mg/kg body weight), respectively. APAP was chosen as a positive control due to its well established hepatotoxicity (Heldring et al., 2022). The results revealed that mice treated with PD-1 DIT did not exhibit elevated ALT and AST levels compared to mice treated with PBS (Figure 6a,b). This conclusion held

true for serum samples collected at 6 h, 24 h, and 48 h after dosing. In contrast, when compared to mice treated with PBS, those treated with APAP had elevated ALT levels at 24 h after dosing (27.5 ± 5.1 vs. 12.9 ± 2.1 , $p < 0.05$) and elevated AST levels at 6 and 24 h after dosing (on average 75.8 ± 6.8 vs. 51.6 ± 5.6 , $p < 0.05$; 77.2 vs. 46.1 , $p < 0.01$). These results suggest that PD-1 DIT does not induce acute hepatotoxicity at its half MTD.

This conclusion is further supported by histological analysis of livers collected from the three groups of mice. There were no discernible morphological differences between the livers of mice treated with PBS and those treated with PD-1 DIT (Figure 6c). Conversely, livers from mice treated with APAP frequently exhibited obvious shrinkage of nuclei, coagulation necrosis near portal triads, and thrombosis in portal veins. Overall, it can be inferred from these results that PD-1 DIT does not cause acute hepatotoxicity.

3 | DISCUSSION

PD-1⁺ lymphocytes have been implicated in the development of autoimmune diseases (Hosseinzadeh et al., 2021; Ivanchenko et al., 2019; Xu et al., 2017). Clinical evidence has shown a significant increase in PD-1⁺ cells in patients with systemic lupus erythematosus (SLE) or RA (Dolff et al., 2014; Lin et al., 2019; Luo et al., 2018). Furthermore, our previous data demonstrated that depletion of PD-1⁺ lymphocytes suppressed or reversed the disease progression (Zhao et al., 2019). Moreover, there is ongoing debate on the role of PD-1⁺ tumor cells in cancer immunity and the resistance to PD-1 immune checkpoint therapy (Du et al., 2018; Kleffel et al., 2015; Wang et al., 2020; Wartewig et al., 2017; Yao et al., 2018). Therefore, it is intriguing to discover roles of PD-1⁺ cells in autoimmune diseases and cancers. Depleting these PD-1⁺ cells could be a powerful approach to define their roles (Wang et al., 2020; Yao et al., 2018). Previously, we created an immunotoxin, α PD-1-ABD-PE, for the depletion that is expressed through *E. coli* system. However, the low yield of the immunotoxin limits its potential as a research tool or therapeutic agent. Hence, it is crucial to develop alternative molecules for PD-1⁺ cell depletion. Using diphtheria toxin as a parent molecule, we generated a new immunotoxin through a yeast expression system, which yields 10 times more than the previous immunotoxin. This yield could be further increased four-fold by transitioning from shake flask culture, currently employed, to a bioreactor (Neville & Liu, 2011). Overall, the improved yield expands the opportunities to study PD-1⁺ cells using cell depletion approach.

PD-1 DIT achieved the same potent level of cytotoxicity as α PD-1-ABD-PE, but with 10 times higher yield. In vitro cytotoxicity assay has shown that EC₅₀ of PD-1 DIT against EL4 and 2D2 cell lines are 0.4 nM and 1.0 nM, respectively. Even though 2D2 cells' PD-1 expression is nearly 4 times lower than EL4's (MFI 23816 vs. MFI 6354), PD-1 DIT is so toxic that the EC₅₀ against 2D2 cells is comparable with EL4 cells. In vivo PD-1⁺ cells depletion studies in the EL4 cells transfer model

further confirmed the potent depletion activity of PD-1 DIT, as the fraction of EL4 cells among T lymphocytes in the bone marrow in PD-1 DIT treated group was significantly lower compared to PBS treated group. Studies on T1D mice models also showed that the number of PD-1⁺ lymphocytes per islet decreased after treatment with PD-1 DIT, compared to PBS treated group. It is noteworthy that majority of PD-1⁺ T lymphocytes are effector cells (Figure S9), which underscores the important role of PD-1⁺ cells in autoimmunity since T effector lymphocytes are recognized as leading cause for autoimmune pathogenesis (Ho & Glimcher, 2002; Jäger & Kuchroo, 2010; Murphy & Reiner, 2002). Preclinical studies with therapeutic purpose showed that after pretreatment with PD-1 DIT, male NOD mice were completely free from T1D while half of the female NOD mice were free from T1D, and the other half had delayed the onset of T1D diabetes. In comparison, all the PBS-pretreated mice developed T1D within 8 days after administration of anti-PD-1 blocking antibodies. The results suggested that the delayed onset of hyperglycemia resulted from the depletion of PD-1⁺ T lymphocytes. Moreover, treatment of PD-1 DIT also relieved SJL/J mice from RR-EAE. Altogether, PD-1 DIT has potent killing effects toward PD-1⁺ lymphocytes while the depletion of PD-1⁺ lymphocytes could lead to the reverse of autoimmune disease progression. In addition to the potent cytotoxicity, PD-1 DIT also possesses the feature of selectivity confirmed by CLSM and MTS assay. The selectivity of PD-1 DIT is of utmost importance to avoid impacting the normal immune response of the body, as is the case with many current treatments. It is acknowledgeable that the treatment of PD-1 DIT results in a reduction of PD-1⁺ cells other than effector cells, such as PD-1⁺ CD44⁺CD62L⁺ T cells. Traditionally, CD44⁺CD62L⁺ T cells are classified as memory cells, however, recent studies have suggested alternative functions and phenotypes of these cells, such as functioning as regulatory T cells (Tregs) or senescent cells (Arata et al., 2019; Arndt et al., 2015; Dai et al., 2010; Shimatani et al., 2009). When considering these CD44⁺CD62L⁺ T cells as Tregs, our data demonstrates that depleting these cells, along with T effector cells, leads to the amelioration of autoimmune diseases. On the other hand, if we regard them as memory T cells, depleting them may have a potential impact on memory immunity. Nevertheless, this impact is likely to be limited because the majority of CD44⁺CD62L⁺ T cells are PD-1⁻ (Figure S8B), and these PD-1⁻ cells can still retain immune memory (Arndt et al., 2015; Dai et al., 2010; Hale & Ahmed, 2015). In addition, memory B cells can sustain important immune memory as well. If compared with other approved therapeutics such as teplizumab (LeFevre et al., 2022) and ocrelizumab (Achiron

et al., 2021; Brill et al., 2021), which affect all T cells and B cells, including memory cells, the depletion of PD-1⁺ cells has a significantly more restricted impact on healthy immune cells. This targeted approach offers a crucial advantage, as it minimizes on-target side effects and enhances the overall safety profile of this strategy. In summary, PD-1 DIT demonstrates both selective and potent cytotoxicity toward PD-1⁺ cells. The depletion of PD-1⁺ lymphocytes holds the potential to alleviate disease progression in both T1D and RR-EAE animal models.

Decades of studies on immunotoxin-based therapies have revealed that the side effects limit their therapeutic potential. Among all the side effects in the immunotoxin-based therapies, the most prevalent is hepatotoxicity, which is due to the binding of basic residues on the variable fragments to negatively charged hepatic cells (Aruna, 2006). Clinical applications of diphtheria toxin-derived immunotoxin, DT388GMCSF and DAB389EGF, have been halted due to their toxicity as both resulted in elevated AST/ALT levels and liver injuries (Shafiee et al., 2019). Hence, we investigated whether PD-1 DIT would cause hepatotoxicity. The results of AST/ALT analysis and Immunohistochemistry results showed no signs of liver injury to mice treated with half MTD of PD-1 DIT. In comparison, acetaminophen treated mice showed significantly higher AST/ALT levels as well as severe liver necrosis. The results indicated that half MTD of PD-1 DIT (0.375 mg/kg) will not cause hepatotoxicity to mice. This dose is dozens of folds higher than DT388GMCSF or DAB389EGF, which both caused hepatotoxicity in clinical trials (5 µg/kg/day and 6 µg/kg/day, respectively) (Shafiee et al., 2019). Altogether, according to the AST/ALT level change and immunohistochemistry results, the half-MTD dose (0.375 mg/kg) of PD-1 DIT is safe to mice.

4 | CONCLUSIONS

PD-1 DIT represents a practical molecular tool for depleting PD-1⁺ cells. It exhibits specific internalization into PD-1⁺ cells and effectively eliminates these cells both in vitro and in vivo. By utilizing this tool, we have discovered that depleting PD-1⁺ lymphocytes in T1D and RR-EAE can effectively reverse the progression of these diseases. Furthermore, administering PD-1 DIT at half of its maximum tolerated dose to C57BL/6 mice does not induce liver damage, indicating its safety for preclinical investigations. In conclusion, PD-1 DIT demonstrates high specificity and potent cytotoxicity, making it a promising candidate for the treatment of autoimmune diseases.

5 | MATERIALS AND METHODS

5.1 | Mice, cell lines and antibodies

Male and female NOD mice, female SJL/J mice and female C57BL/6 mice were purchased from the Jackson Laboratories for the study. All animal experiments were conducted in accordance with the approved protocol by the Institutional Animal Care and Use Committee (IACUC) at the University of Utah. EL4 (ATCC[®] TIB-39[™]) cells were purchased from ATCC and maintained in Dulbecco's Modified Eagle's Medium (DMEM) with 10% horse serum. EL4 (PD-1^{KO}) cells were generated as previously described (Zhao et al., 2019) and maintained in the same medium as EL4 cells. 2D2 cells were a kind gift from Dr. Zemin Zhou and maintained in DMEM with 10% fetal bovine serum (FBS). Antibodies include: FITC anti-mouse CD3 (clone: 17A2), PE anti-mouse TCR Vβ12 (clone: MR11-1), BV510 anti-mouse CD4 (clone: RM4-5), APC/Cyanine7 anti-mouse CD8 (clone: 53-6.7), APC anti-mouse PD-1 (homemade), PerCP/Cyanine5.5 anti-mouse CD19 (clone: 6D5), PE anti-mouse CD62L (clone: W18021D), PE/cyanine7 anti-mouse/human CD44 (clone: IM7).

5.2 | Generation of expression vectors for PD-1 DIT

Genes that encode PD-1 DIT were synthesized by Genewiz and were subsequently inserted into the pPICZα B vectors at the XhoI and XbaI restriction sites. The structure of the PD-1 DIT configuration consists of NH₂-truncated diphtheria toxin-GGGGS-V_H-(GGGGS)₃-V_L-(GGGGS)₃-V_H-(GGGGS)₃-V_L-COOH, where V_H represents the variable regions of the anti-mouse PD-1 heavy chain and V_L represented the anti-mouse PD-1 light chain, respectively. The linker used to connect the light chain and heavy chain in anti-mouse PD-1 scFvs was (GGGGS)₃. Additionally, a GGGGS linker was employed to connect the truncated diphtheria domain with the anti-PD-1 scFvs domain. To facilitate the purification, a 6× Histidine tag (his tag) was added at the C-terminus of PD-1 DIT. The GGGGS linker was inserted between the anti-PD-1 scFvs and the 6× his tag. The sequences of the genes were verified by DNA Sanger sequencing (Genewiz).

5.3 | DNA gel electrophoresis

2 µg PD-1 DIT DNA was double digested by 1 µL of XhoI and 1 µL of XbaI enzyme along with 5 µL of rCutSmart

buffer in a 50 μ L reaction. The digestion reaction was carried out at 37°C for 4 h. Following digestion, 10 μ L of loading dye (6 \times) was added to each sample, and they were subsequently loaded into the wells of 1% DNA agarose gel. Electrophoresis was performed at 120 V for 60 min to separate the DNA fragments. The DNA agarose gel images were captured using the FluorChem FC2 imaging system.

5.4 | Strains and growth conditions

Pichia pastoris Yeast Strain GS115 was purchased from Fisher Scientific. The strains were cultured at 30°C in various growth media, namely YPD medium (consisting of 1% yeast extract, 2% peptone and 2% dextrose), YPG medium (comprising 1% yeast extract, 2% peptone and 1% glycerol), or BMMYC medium (containing 1% yeast extract, 2% peptone, 1% acid casein peptone, 0.67% Yeast Nitrogen Base without amino acids, 4*10⁻⁵% biotins, 0.5% methanol and 1 mM PMSF).

5.5 | Transformation, expression, and purification

The pPICZ α B vectors harboring coding sequences of PD-1 DIT were transformed into the GS115 cells using a chemical method. Initially, a 50 mL culture of GS115 was cultured at 30°C with shaking to an optical density (OD₆₀₀) of 0.8–1.0. The cells were then harvested, washed with 25 mL of sterile water and centrifuged at 1500 g for 10 min at room temperature. The water was discarded, and the cells were resuspended in 1 mL of 100 mM LiCl. Subsequently, the cell suspension was transferred to a microcentrifuge tube and centrifuged at maximum speed for 15 s to remove the LiCl. The cells were then resuspended in 400 μ L of 100 mM LiCl. For each transformation, a 50 μ L aliquot of the cell suspension was transferred to a microcentrifuge tube.

To prepare for the transformation, single-stranded DNA (Herring Sperm DNA) was boiled for 5 min and chilled on ice for later use. pPICZ α B vectors encoding PD-1 DIT sequences were linearized by the SacI restriction enzyme. The 50 μ L aliquoted LiCl-cell solution was centrifuged and the LiCl was removed. The following reagents were added sequentially to the tube: 240 μ L 50% PEG; 36 μ L 1 M LiCl; 25 μ L 2 mg/mL single-stranded DNA; linearized DNA products (5–10 μ g) in 50 μ L sterile water. The tube was vortexed to ensure homogenization of the cell pellet mixture, followed by incubation.

A heat shock was conducted in the water bath at 42°C for 20 min. Then the tubes were centrifuged

at 6000–8000 rpm and the solution was aspirated. The cell pellet was resuspended in 0.5 mL of YPD medium and incubated at 30°C with shaking at 250 rpm. After 4 h, the cell culture was inoculated on YPD plates containing zeocin. Following incubation for 2–3 days at 30°C, colonies were selected and streaked onto a new plate for further purification.

For protein expression, a single colony was selected from the plate and inoculated into 50 mL of YPD medium. The cell culture was then incubated at 30°C with shaking at 250 rpm. Subsequently, 50 mL of the seed culture was transferred to shake flasks containing 1 L YPD medium and culture at 30°C with shaking at 250 rpm for 24 h. After incubation, the cells were centrifuged at 1500 rpm for 15 min at 24°C. The resulting cell pellet was then resuspended in 1 L of YPG medium and cultured at 30°C with shaking at 250 rpm for 24 h. Following this, the cells were centrifuged again at 1500 rpm for 15 min at 24°C. The pellet obtained was resuspended in 500 mL of BMMYC medium and induced at 24°C with shaking at 225 rpm for 48 h. To maintain the concentration of methanol, 2.5 mL (0.5%) methanol was added twice a day during the induction period.

For protein purification, the cell culture was centrifuged by 4000 rpm in a precooled centrifuge at 4°C for 30 min. The resulting supernatant was transferred into a beaker equipped with a stirring bar. The percentage of ammonium sulfate (58%) for protein precipitation was calculated using information from the encorbio website. Gradually, ammonium sulfate was added to the supernatant to precipitate the protein. Simultaneously, 10 M sodium hydroxide solution was gradually added to maintain the pH around 7.4. The solutions were incubated overnight. After incubation, the supernatant was transferred to 50 mL tubes and spun at 7000 g, 4°C for 20 min. The resulting pellet was resuspended in 1 mL PBS for each tube. The mixture was then transferred into dialysis tubing, with 1 mM PMSF (final concentration) being added. The protein mixture was dialyzed for 2 days. For purification, Ni-NTA agarose (Genesee scientific) was used. The protein bound to the agarose was eluted using a 300 mM imidazole solution. The elution was subsequently washed and concentrated using Centrifugal filter units (Sigma–Aldrich, 30 K). The yield and purity of the purified protein was examined using both nonreducing and reducing SDS-PAGE.

5.6 | Size exclusion chromatography

The purity of PD-1 DIT was confirmed using size exclusion chromatography (SEC) on an AKTAFPLC system with a Superdex™ 200 10/300 GL column. The eluent

was PBS at pH 7.4 and the flow rate was set to 0.4 mL/min. To determine the molecular weight of the protein, a Gel Filtration Markers Kit for Protein Molecular Weights (12–200 kD, MWGF200-1KT) was purchased from Sigma–Aldrich.

5.7 | Cellular binding and internalization studies by flow cytometry

PD-1 DIT was labeled with Alexa Fluor 647 NHS Ester (A20006, Thermo Fisher Scientific) as the first step. Subsequently, 1×10^5 EL4 cells were incubated with either 1 μ g/mL or 2.5 μ g/mL Alexa Fluor 647-labeled PD-1 DIT for 0.5 h, 2 h and 4 h at either 4°C or 37°C. Following the incubation, the EL4 cells were stained with DAPI and analyzed using the BD FACS Canto II flow cytometry system (BD Biosciences, San Jose, CA). The mean fluorescence intensity (MFI) of the cells was analyzed and reported.

5.8 | Cell-based direct binding assay

In this experiment, 2×10^5 EL4 or 2D2 cells in 100 μ L were incubated with various concentrations of Alexa Fluor 647-labeled PD-1 DIT for 0.5 h at 4°C. Following the incubation, the cells were washed with FACS buffer (PBS with 0.1% fetal bovine serum) and centrifuged at 300 g for 5 min. After two washes, cells were stained with DAPI and analyzed using flow cytometry to determine the fraction of PD-1⁺ EL4 or 2D2 cells. The fraction of PD-1⁺ cells were plotted against the concentration of free PD-1 DIT, and K_d values were determined by fitting the curve using a sigmoidal dose–response (variable slope) in GraphPad Prism 9. The equation used for fitting the curve was $\text{fraction} = \frac{[L]}{K_d + [L]}$ (Hunter & Cochran, 2016), where $[L]$ represents the concentration of the free PD-1 DIT. The binding avidity is defined as the EC₅₀ of the curve. The 95% confidence intervals were calculated using the GraphPad software.

5.9 | Cellular binding and internalization studies by confocal laser scanning microscopy (CLSM)

In this experiment, 100 μ L of a cell suspension containing 5×10^6 cells/mL of either EL4 or EL4 (PD-1^{KO}) cells were incubated with 100 μ L 1 μ g/mL Alexa Fluor 647 labeled PD-1 DIT for 0.5 h, 2 h, and 10 h in DMEM. To prevent nonspecific binding, 1% FBS was added to the medium. The process of cell adhesion process was

followed as before (Tsang et al., 2017). To stain the cell membrane after cell attachment on coverslips, 5 μ g/mL of WGA555 (ThermoFisher) was used. The cells were incubated with WGA555 for 10 min at 37°C, then washed with PBS for 5 min twice, and fixed with 4% paraformaldehyde (PFA) for 15 min at room temperature. After fixation, the cells were washed with PBS three times. The nuclei were stained with DAPI for 10 min at room temperature, followed by another round of washing. One drop of mounting medium (Fluoromount-G) was placed at the center of the microscope slides. Using Sharp-tipped tweezers, the coverslip with cell facing down was carefully placed onto the mounting medium. After drying for 15 min, nail oil was applied to seal the sides of the coverslips. All the cells were imaged using a Zeiss 700 confocal microscope with a 63 \times oil lens, using the same settings for each channel. The mean intensity value of Alexa Fluor 647 labeled PD-1 DIT signal on each cell was quantified using the ZEN 3.6 edition software.

To quantify the mean intensity value, the fluorescence signal from each cell was meticulously enclosed with a circle (shown in Figure S6), and the software calculated the resulting signal intensities. All the intensity values from each cell were collected and were analyzed by GraphPad Prism 9.

5.10 | In vitro cytotoxicity study

EL4, EL4 (PD-1^{KO}) or 2D2 cell lines were seeded at a density of 4000 cells per well in a 96-well plate. The cells were then incubated with PD-1 DIT at various dilutions for either 24 or 72 h. Following the incubation period, cell proliferation was assessed using the CellTiter assay (Promega), and the absorbance at 490 nm was measured for each sample. The experimental setup also included a negative control group treated with 1% Triton X-100 and a positive control group treated with PBS. The cell viability data was processed and analyzed using GraphPad Prism 9. The data was fitted to a Sigmoidal dose–response (variable slope) curve to determine the EC₅₀ value, which represents the concentration of PD-1 DIT that inhibits 50% of cell proliferation.

5.11 | In vivo PD-1⁺ cells depletion study

On Day 0, C57BL/6 mice were intravenously injected with 3×10^6 of EL4 cells. The mice were randomly divided into two treatment groups: one group received intravenous injections (i.v.) of 0.15 mg/kg PD-1 DIT, while the other group received PBS as a control. Each group consisted of five treated mice. The injections were

administered every 2 days, 5 doses in total. On Day 12, the mice were euthanized, and cells were collected from bone marrow and blood. The collected cells were then stained with BV510 anti-mouse CD4, APC/Cy7 anti-mouse CD8, APC anti-mouse PD-1, FITC anti-mouse CD3 and PE anti-mouse TCR V β 12 antibodies. Flow cytometry analysis was performed using the BD FACS CANTO II flow cytometer (BD Biosciences, San Jose, CA). The fraction of PD-1⁺ cells among T cells was quantified to assess the depletion of PD-1⁺ cells in response to the treatment.

For survival study, on Day 0, 2*10⁴ EL4 cells were intravenously injection into 10 female C57BL/6 mice. The mice were then randomly divided into two groups. From Day 1, the two groups received a total of five doses treatment every 2 days, through i.v. injection. One group received 0.15 mg/kg of PD-1 DIT for each dose, while the other group received PBS as a control. Throughout the study, the survival days of the mice were monitored and recorded.

Ten female NOD mice, 10-week-old, were randomly divided into two groups. From Day 0 to Day 3, one group received daily treatment with 0.15 mg/kg PD-1 DIT, while the other group received daily PBS treatment as a control. On Day 5, mice were euthanized, and islets were collected. The collected islets were stained with FITC anti-mouse CD3, BV510 anti-mouse CD4, APC/Cy7 anti-mouse CD8, PerCP/Cy5.5 anti-mouse CD19, PE anti-mouse CD62L, PE/Cy7 anti-mouse CD44, APC anti-mouse PD-1 antibodies and Alexa Fluor 405-DAPI. Flow cytometry analysis was performed using the BD FACS CANTO II flow cytometer (BD Biosciences, San Jose, CA). The number of PD-1⁺ cells per islet was quantified to assess the depletion of PD-1⁺ cells.

5.12 | T1D study

Sixteen NOD mice, consisting of 8 females and 8 males, were randomly divided into 4 groups based on their gender. One group from each gender were pretreated with 0.15 mg/kg PD-1 DIT while the other group from each gender were pretreated with PBS as a control. The mice received a total of 5 intraperitoneal (i.p.) doses, administered every 2 days. Starting from day 0, the mice were also given 250 μ g of blocking anti-mouse PD-1 antibodies i.p., for a total of 5 doses administered every 2 days. Throughout the experiment, blood glucose levels of the mice were monitored using a Contour Next EZ Blood Glucose Meter (Amazon). The onset of T1D was confirmed for a mouse when its blood glucose concentration exceeded 250 mg/dL for two continuous measurements. To assess the impact of the treatments on diabetes onset,

diabetes-free survival was analyzed using GraphPad Prism 9.

5.13 | RR-EAE study

Thirty female SJL/J mice were randomly divided into two groups. On day 0, they were immunized with a peptide of proteolipid-protein (139–151) homogenized by 0.2 mL complete Freund's adjuvant (CFA) from Sigma. The mice received 4 subcutaneous injections of peptides on theirs, with a total of 50 μ g per mouse. On day 3, the two groups of mice were treated i.p. with either 0.15 mg/kg PD-1 DIT or PBS. The treatment was administered for a total of 5 doses, with each dose given every other day. Throughout the experiment, the mice's body weight and the presence of paralysis symptoms were monitored every other day. Clinical scores were assigned to each mouse based on the severity of the paralysis observed.

5.14 | Hepatotoxicity assessment

On day 0, 15 female C57BL/6 mice at 10 weeks of age were weighed and randomly assigned into 3 groups. The groups were administered 450 mg/kg acetaminophen, 0.375 mg/kg PD-1 DIT, or PBS through i.p., respectively. After 6 h, 24 h, and 48 h, blood samples were collected from the cheek of each mouse. At the end of the study, which was at 48 h, mice were euthanized. Liver samples were collected for immunohistochemistry analysis, and liver paraffin sections were stained with H&E. Serum ALT/AST activity was measured using a colorimetric method specifically designed for ALT/AST analysis (BIOLABO).

5.15 | Statistical analysis

Unpaired two-sided *t*-test were used to compare data other than survival data. The survival curves are calculated from different treatment groups using the Kaplan–Meier estimation approach and their difference was compared using a log-rank test. The level of test significance was defined as *p*-value <0.05. The survival analyses were conducted using GraphPad Prism 9.

AUTHOR CONTRIBUTIONS

Tianxiao Zhang: Conceptualization, methodology, investigation, data analysis, writing—original draft. **Shuyun Dong:** Conceptualization, methodology, investigation, data analysis, writing-review & editing. **Yujia Zhai:** Methodology, investigation. **Lauren Naatz:**

Methodology, review & editing. **Zemin Zhou:** Investigation. **Mingnan Chen:** Conceptualization, investigation, writing-review & editing, supervision, funding acquisition.

ACKNOWLEDGMENTS

We recognize Core Facility of University of Utah for the service with Flow cytometry and confocal laser scanning chromatography. We appreciate Dr. Shawn Owen's assistance for the generation of protein structure. We appreciate Dr. Jane Yang's help for performing size exclusion chromatography. We appreciate Dr. Xiang Wang help for confocal imaging study. We recognize ARUP lab for the service of immunohistochemistry. We appreciate Dr. Shihai Jia and Dr. Jianmin Zhang's help for liver histology.

FUNDING INFORMATION

The work was primarily supported by the HCI Melanoma Center Grant, the National Institutes of Health AI139535 grant, and the National Multiple Sclerosis Society GR-1807-31630 grant to M.C.

CONFLICT OF INTEREST STATEMENT

The authors have declared that no competing interest exists.

DATA AVAILABILITY STATEMENT

All data generated or analyzed during this study are included in this published article and its supplementary information files.

INFORMED CONSENT

All authors agree to submit the manuscript for publication.

ORCID

Mingnan Chen  <https://orcid.org/0000-0002-7080-9804>

REFERENCES

- Achiron A, Mandel M, Dreyer-Alster S, Harari G, Magalashvili D, Sonis P, et al. Humoral immune response to COVID-19 mRNA vaccine in patients with multiple sclerosis treated with high-efficacy disease-modifying therapies. *Ther Adv Neurol Disord*. 2021;14:17562864211012835.
- Ansari MJI, Salama AD, Chitnis T, Smith RN, Yagita H, Akiba H, et al. The programmed death-1 (PD-1) pathway regulates auto-immune diabetes in nonobese diabetic (NOD) mice. *J Exp Med*. 2003;198(1):63–9.
- Arata Y, Watanabe A, Motosugi R, Murakami R, Goto T, Hori S, et al. Defective induction of the proteasome associated with T-cell receptor signaling underlies T-cell senescence. *Genes Cells*. 2019;24(12):801–13.
- Arndt Br, Witkowski L, Ellwart J, Seissler J. CD8+ CD122+ PD-1–effector cells promote the development of diabetes in NOD mice. *J Leucocyte Biol*. 2015;97(1):111–20.
- Aruna G. Immunotoxins: a review of their use in cancer treatment. *J Stem Cells Regen Med*. 2006;1(1):31–6.
- Auger A, Park M, Nitschke F, Minassian LM, Beilhardt GL, Minassian BA, et al. Efficient delivery of structurally diverse protein cargo into mammalian cells by a bacterial toxin. *Mol Pharm*. 2015;12(8):2962–71.
- Becker N, Benhar I. Antibody-based immunotoxins for the treatment of cancer. *Antibodies*. 2012;1(1):39–69.
- Bennett M, Choe S, Eisenberg D. Refined structure of dimeric diphtheria toxin at 2.0 Å resolution. *Protein Sci*. 1994;3(9):1444–63.
- Brill L, Rechtman A, Zveik O, Haham N, Oiknine-Djian E, Wolf DG, et al. Humoral and T-cell response to SARS-CoV-2 vaccination in patients with multiple sclerosis treated with ocrelizumab. *JAMA Neurol*. 2021;78(12):1510–4.
- Chen J, Bodley J, Livingston DM. Diphtheria toxin-resistant mutants of *Saccharomyces cerevisiae*. *Mol Cell Biol*. 1985;5(12):3357–60.
- Collier R. Understanding the mode of action of diphtheria toxin: a perspective on progress during the 20th century. *Toxicon*. 2001;39(11):1793–803.
- Cregg JM, Barringer KJ, Hessler AY, Madden KR. *Pichia pastoris* as a host system for transformations. *Mol Cell Biol*. 1985;5(12):3376–85.
- Dai H, Wan N, Zhang S, Moore Y, Wan F, Dai Z. Cutting edge: programmed death-1 defines CD8+ CD122+ T cells as regulatory versus memory T cells. *J Immunol*. 2010;185(2):803–7.
- Dolff S, Quandt D, Feldkamp T, Jun C, Mitchell A, Hua F, et al. Increased percentages of PD-1 on CD4+ T cells is associated with higher INF-γ production and altered IL-17 production in patients with systemic lupus erythematosus. *Scand J Rheumatol*. 2014;43(4):307–13.
- Du S, McCall N, Park K, Guan Q, Fontina P, Ertel A, et al. Blockade of tumor-expressed PD-1 promotes lung cancer growth. *Onco Targets Ther*. 2018;7(4):e1408747.
- Fife BT, Guleria I, Gubbels Bupp M, Eagar TN, Tang Q, Bour-Jordan H, et al. Insulin-induced remission in new-onset NOD mice is maintained by the PD-1–PD-L1 pathway. *J Exp Med*. 2006;203(12):2737–47.
- Fife BT, Pauken KE, Eagar TN, Obu T, Wu J, Tang Q, et al. Interactions between PD-1 and PD-L1 promote tolerance by blocking the TCR-induced stop signal. *Nat Immunol*. 2009;10(11):1185–92.
- Gellissen G. Heterologous protein production in methylotrophic yeasts. *Appl Microbiol Biotechnol*. 2000;54(6):741–50.
- Hale JS, Ahmed R. Memory T follicular helper CD4 T cells. *Front Immunol*. 2015;6:16.
- Hammer LA, Zagon IS, McLaughlin PJ. Treatment of a relapse-remitting model of multiple sclerosis with opioid growth factor. *Brain Res Bull*. 2013;98:122–31.
- Hao H, Nakayamada S, Tanaka Y. Differentiation, functions, and roles of T follicular regulatory cells in autoimmune diseases. *Inflamm Regen*. 2021;41(1):1–8.
- Heldring M, Shaw AH, Beltman JB. Unraveling the effect of intra-and intercellular processes on acetaminophen-induced liver injury. *npj Syst Biol Appl*. 2022;8(1):1–16.

- Ho I-C, Glimcher LHJC. Transcription: tantalizing times for T cells. *Cell*. 2002;109(2):S109–20.
- Hosseinzadeh R, Feizisani F, Shomali N, Abdelbasset WK, Hemmatzadeh M, Gholizadeh Navashenaq J, et al. PD-1/PD-L1 blockade: prospectives for immunotherapy in cancer and autoimmunity. *IUBMB Life*. 2021;73(11):1293–306.
- Huang Y, Chen Z, Wang H, Ba X, Shen P, Lin W, et al. Follicular regulatory T cells: a novel target for immunotherapy? *Clin Transl Immunol*. 2020;9(2):e1106.
- Hunter S, Cochran J. Cell-binding assays for determining the affinity of protein–protein interactions: technologies and considerations. *Methods Enzymol*. 2016;580:21–44.
- Ishida YJC. PD-1: its discovery, involvement in cancer immunotherapy, and beyond. *Cells*. 2020;9(6):1376.
- Ivanchenko M, Aqrabi LA, Björk A, Wahren-Herlenius M, Chemin K. FoxP3+ CXCR5+ CD4+ T cell frequencies are increased in peripheral blood of patients with primary Sjögren's syndrome. *Clin Exp Immunol*. 2019;195(3):305–9.
- Jäger A, Kuchroo VKJSjoi. Effector and regulatory T-cell subsets in autoimmunity and tissue inflammation. *Scand J Immunol*. 2010;72(3):173–84.
- Joller N, Peters A, Anderson AC, Kuchroo VK. Immune checkpoints in central nervous system autoimmunity. *Immunol Rev*. 2012;248(1):122–39.
- Kleffel S, Posch C, Barthel SR, Mueller H, Schlapbach C, Guenova E, et al. Melanoma cell-intrinsic PD-1 receptor functions promote tumor growth. *Cell*. 2015;162(6):1242–56.
- LeFevre JB, Cyriac SL, Tokmic A, Pitlick JM. Anti-CD3 monoclonal antibodies for the prevention and treatment of type 1 diabetes: a literature review. *Am J Health Syst Pharm*. 2022;79(23):2099–117.
- Li H, Li X, Liu S, Guo L, Zhang B, Zhang J, et al. Programmed cell death-1 (PD-1) checkpoint blockade in combination with a mammalian target of rapamycin inhibitor restrains hepatocellular carcinoma growth induced by hepatoma cell-intrinsic PD-1. *Hepatology*. 2017;66(6):1920–33.
- Liang SC, Latchman YE, Buhlmann JE, Tomczak MF, Horwitz BH, Freeman GJ, et al. Regulation of PD-1, PD-L1, and PD-L2 expression during normal and autoimmune responses. *Eur J Immunol*. 2003;33(10):2706–16.
- Lin J, Yu Y, Ma J, Ren C, Chen W. PD-1+ CXCR5– CD4+ T cells are correlated with the severity of systemic lupus erythematosus. *Rheumatology*. 2019;58(12):2188–92.
- Liu YY, Gordienko I, Mathias A, Ma S, Thompson J, Woo JH, et al. Expression of an anti-CD3 single-chain immunotoxin with a truncated diphtheria toxin in a mutant CHO cell line. *Protein Expr Purif*. 2000;19(2):304–11.
- Luo Q, Ye J, Zeng L, Luo Z, Deng Z, Li X, et al. Elevated expression of PD-1 on T cells correlates with disease activity in rheumatoid arthritis. *Mol Med Rep*. 2018;17(2):3297–305.
- Mei X, Chen J, Wang J, Zhu J. Immunotoxins: targeted toxin delivery for cancer therapy. *Pharm Fronts*. 2019;1(1):e33–45.
- Mirdita M, Schütze K, Moriwaki Y, Heo L, Ovchinnikov S, Steinegger M. ColabFold: making protein folding accessible to all. *Nat Methods*. 2022;19:679–82.
- Moolten FL, Cooperband SR. Selective destruction of target cells by diphtheria toxin conjugated to antibody directed against antigens on the cells. *Science*. 1970;169(3940):68–70.
- Moore SJ, Cochran JR. Engineering knottins as novel binding agents. *Methods Enzymol*. 2012;503:223–51.
- Murphy KM, Reiner SLJNRI. The lineage decisions of helper T cells. *Nat Rev Immunol*. 2002;2(12):933–44.
- National Multiple Sclerosis Society. Available from. 2013: <https://www.nationalmssociety.org/About-the-Society/MS-Prevalence>
- Neville DM, Woo J-H, Liu Y-Y. Methods for expression and purification of immunotoxins. 2011 Google Patents.
- Nishimura H, Nose M, Hiai H, Minato N, Honjo T. Development of lupus-like autoimmune diseases by disruption of the PD-1 gene encoding an ITIM motif-carrying immunoreceptor. *Immunity*. 1999;11(2):141–51.
- Okazaki T, Chikuma S, Iwai Y, Fagarasan S, Honjo T. A rheostat for immune responses: the unique properties of PD-1 and their advantages for clinical application. *Nat Immunol*. 2013;14(12):1212–8.
- Patsoukis N, Wang Q, Strauss L, Boussiotis VA. Revisiting the PD-1 pathway. *Sci Adv*. 2020;6(38):eabd2712.
- Pauken KE, Torchia JA, Chaudhri A, Sharpe AH, Freeman GJ. Emerging concepts in PD-1 checkpoint biology. *Semin Immunol*. 2021;52:101480.
- Perentesis JP, Genbauffe FS, Veldman SA, Galeotti CL, Livingston DM, Bodley JW, et al. Expression of diphtheria toxin fragment A and hormone-toxin fusion proteins in toxin-resistant yeast mutants. *Proc Natl Acad Sci U S A*. 1988; 85(22):8386–90.
- Reiter Y, Pai LH, Brinkmann U, Wang QC, Pastan I. Antitumor activity and pharmacokinetics in mice of a recombinant immunotoxin containing a disulfide-stabilized Fv fragment. *Cancer Res*. 1994;54(10):2714–8.
- Salama AD, Chitnis T, Imitola J, Ansari MJI, Akiba H, Tushima F, et al. Critical role of the programmed death-1 (PD-1) pathway in regulation of experimental autoimmune encephalomyelitis. *J Exp Med*. 2003;198(1):71–8.
- Salaspuro MJE. Use of enzymes for the diagnosis of alcohol-related organ damage. *Enzyme*. 1987;37:87–107.
- Schatton T, Schütte U, Frank NY, Zhan Q, Hoerning A, Robles SC, et al. Modulation of T-cell activation by malignant melanoma initiating cells. *Cancer Res*. 2010;70(2):697–708.
- Shafiee F, Aucoin MG, Jahanian-Najafabadi A. Targeted diphtheria toxin-based therapy: a review article. *Front Microbiol*. 2019;10:2340.
- Shapira A, Benhar I. Toxin-based therapeutic approaches. *Toxins*. 2010;2(11):2519–83.
- Shimatani K, Nakashima Y, Hattori M, Hamazaki Y, Minato N. PD-1+ memory phenotype CD4+ T cells expressing C/EBP α underlie T cell immunodepression in senescence and leukemia. *Proc Natl Acad Sci U S A*. 2009;106(37):15807–12.
- Thompson J, Stavrou S, Weetall M, Hexham JM, Digan ME, Wang Z, et al. Improved binding of a bivalent single-chain immunotoxin results in increased efficacy for in vivo T-cell depletion. *Protein Eng*. 2001;14(12):1035–41.
- Tsang M, Gantchev J, Ghazawi FM, Litvinov IV. Protocol for adhesion and immunostaining of lymphocytes and other non-adherent cells in culture. *Biotechniques*. 2017;63(5):230–3.
- Varkouhi AK, Scholte M, Storm G, Haisma HJ. Endosomal escape pathways for delivery of biologicals. *J Control Release*. 2011; 151(3):220–8.

- Wang X, Yang X, Zhang C, Wang Y, Cheng T, Duan L, et al. Tumor cell-intrinsic PD-1 receptor is a tumor suppressor and mediates resistance to PD-1 blockade therapy. *Proc Natl Acad Sci U S A*. 2020;117(12):6640–50.
- Wang Z, Zheng Q, Zhang H, Bronson RT, Madsen JC, Sachs DH, et al. Ontak-like human IL-2 fusion toxin. *J Immunol Methods*. 2017;448:51–8.
- Wartewig T, Kurgys Z, Keppler S, Pechloff K, Hameister E, Öllinger R, et al. PD-1 is a haploinsufficient suppressor of T cell lymphomagenesis. *Nature*. 2017;552(7683):121–5.
- Williams D, Parker K, Bacha P, Bishai W, Borowski M, Genbauffe F, et al. Diphtheria toxin receptor binding domain substitution with interleukin-2: genetic construction and properties of a diphtheria toxin-related interleukin-2 fusion protein. *Protein Eng*. 1987;1(6):493–8.
- Woo JH, Liu YY, Mathias A, Stavrou S, Wang Z, Thompson J, et al. Gene optimization is necessary to express a bivalent anti-human anti-T cell immunotoxin in *Pichia pastoris*. *Protein Expr Purif*. 2002;25(2):270–82.
- Xie MM, Fang S, Chen Q, Liu H, Wan J, Dent AL. Follicular regulatory T cells inhibit the development of granzyme B-expressing follicular helper T cells. *JCI Insight*. 2019;4(16):e128076.
- Xu B, Wang S, Zhou M, Huang Y, Fu R, Guo C, et al. The ratio of circulating follicular T helper cell to follicular T regulatory cell is correlated with disease activity in systemic lupus erythematosus. *Clin Immunol*. 2017;183:46–53.
- Yao H, Wang H, Li C, Fang JY, Xu J. Cancer cell-intrinsic PD-1 and implications in combinatorial immunotherapy. *Front Immunol*. 2018;9:1774.
- Young EF, Hess PR, Arnold LW, Tisch R, Frelinger JA. Islet lymphocyte subsets in male and female NOD mice are qualitatively similar but quantitatively distinct. *Autoimmunity*. 2009;42(8):678–91.
- Zhai Y, Dong S, Li H, Zhang Y, Shami P, Chen M. Antibody-mediated depletion of programmed death 1-positive (PD-1+) cells. *J Control Release*. 2022;349:425–33.
- Zhao P, Wang P, Dong S, Zhou Z, Cao Y, Yagita H, et al. Depletion of PD-1-positive cells ameliorates autoimmune disease. *Nat Biomed Eng*. 2019;3(4):292–305.
- Zhou H, Hu B, Zhaopeng Z, Liu J, Zhong Q, Fan Y, et al. Elevated circulating T cell subsets and cytokines expression in patients with rheumatoid arthritis. *Clin Rheumatol*. 2019;38(7):1831–9.

SUPPORTING INFORMATION

Additional supporting information can be found online in the Supporting Information section at the end of this article.

How to cite this article: Zhang T, Dong S, Zhai Y, Naatz L, Zhou Z, Chen M. Diphtheria toxin-derived, anti-PD-1 immunotoxin, a potent and practical tool to selectively deplete PD-1⁺ cells. *Protein Science*. 2023;32(9):e4741. <https://doi.org/10.1002/pro.4741>